Bioelectrochemistry 138 (2021) 107695

Contents lists available at ScienceDirect

Bioelectrochemistry

journal homepage: www.elsevier.com/locate/bioelechem

Electrochemical sensor for selective tyramine determination, amplified by a molecularly imprinted polymer film

Viknasvarri Ayerdurai [a], Maciej Cieplak [a,*], Krzysztof R. Noworyta [a], Marianna Gajda [a,b], Agnieszka Ziminska [a,b], Marta Sosnowska [a], Joanna Piechowska [a], Pawel Borowicz [a], Wojciech Lisowski [a], Shuai Shao [c], Francis D'Souza [c,*], Wlodzimierz Kutner [a,d,*]

[a] Institute of Physical Chemistry, Polish Academy of Sciences, Kasprzaka 44/52, 01-224 Warsaw, Poland
[b] Faculty of Pharmacy with Laboratory Medicine Division, Medical University of Warsaw, Banacha 1, 02-091 Warsaw, Poland
[c] Department of Chemistry, University of North Texas, Denton, 1155, Union Circle, #305070, TX 76203-5017, USA
[d] Faculty of Mathematics and Natural Sciences. School of Sciences, Cardinal Stefan Wyszynski University in Warsaw, Wóycickiego 1/3, 01-815 Warsaw, Poland

ARTICLE INFO

Article history:
Received 17 March 2020
Received in revised form 30 September 2020
Accepted 7 October 2020
Available online 17 November 2020

Keywords:
Chemosensor
Conductive polymer
Molecularly imprinted polymer, MIP
Food toxin
Tyramine electrochemical sensor

ABSTRACT

A molecularly imprinted polymer (MIP) film based electrochemical sensor for selective determination of tyramine was devised, fabricated, and tested. Tyramine is generated in smoked and fermented food products. Therefore, it may serve as a marker of the rottenness of these products. Importantly, intake of large amounts of tyramine by patients treated with monoamine oxidase (MAO) inhibitors may lead to a "cheese effect", namely, a dangerous hypertensive crisis. The limit of detection at S/N = 3 of the chemosensor, in both differential pulse voltammetry (DPV) and electrochemical impedance spectroscopy (EIS) determinations, with the use of the $Fe(CN)_6^{4-}/Fe(CN)_6^{3-}$ redox probe, was 159 and 168 μM tyramine, respectively. The linear dynamic concentration range was 290 μM to 2.64 mM tyramine. The chemosensor was highly selective with respect to the glucose, urea, and creatinine interferences. Its DPV determined apparent imprinting factor was 5.6. Moreover, the mechanism of the "gate effect" in the operation of the polymer film-coated electrodes was unraveled.

1. Introduction

Tyramine is a typical biogenic primary amine. Living organisms produce it via decarboxylation of tryptophan. Tyramine can be found in smoked and fermented food products. Moreover, it may serve as a marker of the rottenness of these products [1]. Tyramine is mostly used as such for perishable foodstuff, e.g., meat and fish products. Therefore, tyramine determination can be very useful in food quality control.

Tyramine is decomposed by monoamine oxidase (MAO). Intake of large amounts of tyramine by patients treated with MAO inhibitors or antidepressants may lead to the so-called "cheese effect", namely, dangerous hypertensive crisis [2]. Moreover, long-term elevated tyramine levels in the blood may result in hypertension [3]. Therefore, these patients should avoid tyramine containing food, including pickles, cheese, yogurt, fish, and meat products, as well as fruits, including cacao seeds, bananas, avocados, figs, and pineapples. Tyramine contents in representative food products considered to be risky for the patients mentioned above are listed in Table 1 [4]. Procedures for small biogenic amines determination in food products usually involve chromatographic techniques. These procedures are exact and accurate. However, they require relatively expensive instrumentation, experienced operators, and large amounts of costly chemicals. These requirements highlight a high need for developing robust, inexpensive, and easy to handle determination procedures.

Concerning analytical parameters, chemosensors may fulfill the demand indicated above. Therefore, within the present research, we devised, fabricated, and tested an electrochemical chemosensor for selective determination of tyramine. Molecularly imprinted polymer (MIP) film deposited on the electrode surface can ensure selective tyramine recognition [5,6]. Until now, only a few attempts of tyramine imprinting in polymers were reported. Sol-gel systems [7–11] and acrylic polymers [12–14] were imprinted with tyramine. These polymers served as SPE column packing materials [13] or as selective recognition units of optical [10–12] and electrochemical sensors [7–9,14]. Within the above MIP

* Corresponding authors at: Institute of Physical Chemistry, Polish Academy of Sciences, Kasprzaka 44/52, 01-224 Warsaw, Poland (M. Cieplak and W. Kutner) and Department of Chemistry, University of North Texas, Denton, 1155, Union Circle, #305070, TX 76203-5017, USA (F. D'Souza).
E-mail addresses: mcieplak@ichf.edu.pl (M. Cieplak), francis.dsouza@unt.edu (F. D'Souza), wkutner@ichf.edu.pl (W. Kutner).

https://doi.org/10.1016/j.bioelechem.2020.107695
1567-5394/

Table 1
Tyramine content in food products considered not to be recommended for patients treated with MAO inhibitors or antidepressants. Adapted from reference [4].

Food product	Portion size	Tyramine content, mg	Tyramine content, μmol	Tyramine concentration, mM[a]
Canadian cheddar	28 g	43	314	11.2
Camembert cheese	28 g	38	277	9.9
Bleu/Blue cheese	28 g	28	204	4.7
Gorgonzola	28 g	1.6	11	0.42
Cottage cheese, fresh	112 g	0	0	0
Tap beer	355 mL	38	277	0.78
Chicken livers, aged	28 g	60	438	15.6
Sauerkraut	112 g	3.5–14	25–102	0.23 – 0.91
Soy sauce	5 mL	0.05–4.7	3.6–34	0.073–6.86
Thai fish sauce	5 mL	0–3.7	27	5.4

[a] The tyramine concentration was calculated assuming that the food product density is equal to that of water.

chemosensors, direct tyramine electro-oxidation at 0.70 V vs. Ag/AgCl produced faradaic currents. However, these currents were very low [7,8]. Therefore, it was necessary to modify surfaces of electrodes with nanomaterials, including carbon nanotubes, gold nanoparticles, and conductive polymer composites, to reach acceptable chemosensor sensitivity [9,14]. Moreover, for the above-mentioned optical sensors, imprinting factors were small or not reported at all [10–12]. Thus, the efficiency of the reported imprinting methods was limited. Indirect electrochemiluminescence sensing protocol was recently proposed to circumvent these problems [15]. In this protocol, graphitic-phase carbon nitride (g-C_3N_4) nanosheets were deposited on the rGO-COOH support and subsequently coated with the film of poly(*o*-phenylenediamine) imprinted with tyramine. The (carbon nitride nanosheets)/rGO-COOH electrochemiluminescence was quenched because of tyramine binding in the MIP film. The reported chemosensor enabled selective tyramine determination in the 10 nM to 1 mM linear dynamic concentration range. In our present research, we propose a simplified approach to indirect electrochemical tyramine determination using an MIP chemosensor.

In the present research, tyramine was imprinted in a derivatized conductive polythiophene film. The resulting MIP-tyramine film-coated electrodes were applied for selective determination of tyramine using electrochemical transduction techniques in combination with the so-called "gate effect" [16]. Moreover, the mechanism of this effect on the MIP and control non-imprinted (NIP) film-coated electrodes was unraveled.

2. Procedures

2.1. Monomer synthesis

Synthesis of the functional monomer, *p*-bis(2,2′-bithien-5-yl)-methylbenzo-18-crown-6 **FM2**, was described elsewhere [17].

2.2. MIP and NIP films simultaneous synthesizing and depositing

The **MIP-1** film was prepared by oxidative electropolymerization under potentiodynamic conditions involving five potential cycles over the potential range of 0 to 1.30 V vs. Ag quasi-reference electrode at a potential scan rate of 50 mV/s. An acetonitrile solution of 50 μM tyramine, 100 μM 2,2′-bithiophene-5-carboxylic acid **FM1**, 500 μM 2,3′-bithiophene, and 100 mM tetrabutylammonium perchlorate, (TBA)ClO_4, was used for this electropolymerization.

The **MIP-2** film was prepared by oxidative electropolymerization under potentiodynamic conditions within two potential cycles over the potential range of 0 to 1.30 V vs. Ag quasi-reference electrode at a potential scan rate of 50 mV/s. An acetonitrile solution of 50 μM tyramine, 100 μM **FM1**, 50 μM **FM2**, 500 μM 2,3′-bithiophene, and 100 mM (TBA)ClO_4 was used for this electropolymerization.

After electropolymerization, the films were trice rinsed with acetonitrile to remove (TBA)ClO_4 and residues of unreacted monomers. Subsequently, the tyramine template was extracted from the **MIP-1** and **MIP-2** films by immersing the film-coated electrodes in 0.1 M NaOH for 150 min at room temperature, 20 (±1) °C. The **NIP-1** and **NIP-2** control films were prepared by oxidative electropolymerization under the same conditions as those used for the **MIP-1** and **MIP-2** syntheses but in the tyramine absence. Moreover, the **NIP-1** and **NIP-2** films were subjected to the same "extraction" procedures as the **MIP-1** and **MIP-2** films.

Before depositing the MIP and NIP films, the electrodes were cleaned in a "piranha" solution for 10 min, and then mirror finished with 0.05-μm alumina slurry. (*Warning. The "piranha" solution is hazardous if it comes in contact with skin or eye.*)

For XPS and PM-IRRAS measurements as well as AFM imaging, the MIP and NIP films were deposited on Au film-coated, with Ti underlayer, glass slides using a homemade holder with a Pt plate as the counter electrode and an Ag wire as the quasi-reference electrode. The working and counter electrodes were mounted in parallel, face-to-face, at a distance of ~ 5 mm [18].

2.3. Electrochemical measurements

All DPV and EIS measurements were performed at room temperature using the electrochemical mini cell (Section S2 in Supplementary Material), in the 0.1 M phosphate-buffered saline, PBS, (pH = 7.4) solution of the 100 mM $K_3[Fe(CN)_6]$ and 100 mM $K_4[Fe(CN)_6]$ redox probe.

In DPV measurements, the potential was scanned from 0 to 0.60 V vs. Ag quasi-reference electrode with the potential step of 5 mV. The amplitude of 50-ms pulses applied was 25 mV. A drop of the redox probe faradaic current served as the analytical signal [16,19].

In the EIS experiments, an ac excitation signal of frequency in the range of 1 MHz to 100 mHz and 10-mV sinusoidal amplitude was used at a potential of 0.20 V vs. Ag quasi-reference electrode.

After each tyramine determination, the **MIP-1** and **MIP-2** film-coated electrodes were immersed in 0.1 M NaOH for 10 to 150 min, at room temperature, under magnetic stirring, until the analyte was extracted entirely. The extraction completeness was confirmed by a stable DPV peak of ~ 45 μA for the redox probe.

2.4. Preparing Mozzarella cheese whey samples

For the preparation of these samples, a package of Mozzarella cheese of the Galbani Mozzarella company was purchased in a local supermarket. A 35-mL of whey from a freshly opened package of this cheese was collected. Solid contaminants of the whey sample were removed by twice centrifuging (20 min, 10 000 rpm).

Then, the supernatant was collected and twice washed with chloroform (10 mL). Next, the collected aqueous phase was 100 times diluted with deionized water. This solution was divided into two equal portions. To one, the PBS (pH = 7.4) solution of $K_3[Fe(CN)_6]$ and $K_4[Fe(CN)_6]$ redox probe was added to reach the same concentrations as those described in Section 2.3 above. The solutions prepared that way were applied for DPV tyramine determinations in the same way as that described in Section 2.3 above to construct calibration plots.

The other portion was stored in the freezer. Later, it was thawed, and the 0.1 M PBS (pH = 7.4) solution of the $K_3[Fe(CN)_6]$ and $K_4[Fe(CN)_6]$ redox probe was added, as previously. Then, it was divided into four samples, and each of these samples was spiked with a known amount of tyramine. Finally, tyramine was determined in these samples using a freshly prepared **MIP-2** film coated electrode.

3. Results and discussion

3.1. Selecting functional monomers

Functional monomers provide a pattern of interactions that enable selective recognition of the target analyte molecules by the MIP molecular cavities. Therefore, the selection of appropriate functional monomers is one of the most critical issues concerning successful imprinting. The chosen monomers should form a stable, in solution, pre-polymerization complex with the template. Thus, the functional monomers would be placed on expected positions inside of the imprinted cavities after complex copolymerization with a cross-linking monomer and subsequent template removal. For that purpose, the tyramine template complexation with the most promising functional monomers was simulated with DFT. Initially, the **FM1** monomer was selected. Results of the DFT calculations suggested that this monomer could form a stable complex with tyramine of the 2 : 1 M ratio (Scheme 1a and 1b). The monomer **FM1** participated in hydrogen bond formation with the hydroxyl group of tyramine as the acceptor. Moreover, this monomer could bind a protonated primary amine group of tyramine. The calculated Gibbs free energy change due to complex formation was quite appreciable ΔG = -180 kJ/mol. The electrode coated with the film prepared using the **FM1** monomer, indicated as **MIP-1**, was highly sensitive to tyramine. Unfortunately, in subsequent studies described below, this chemosensor appeared nonselective to common interferences (see Figure S3 in Supplementary Material).

Therefore, we searched for another functional monomer, which would be able to provide additional interactions with the tyramine template for higher selectivity. It appeared that the crown-ether-moiety-containing monomer **FM2** fulfilled this requirement. That is, this moiety formed a supramolecular complex with the protonated primary amine group of tyramine. Moreover, one molecule of monomer **FM1** served as the counterion, thus neutralizing the positive charge on the above protonated primary amine group of tyramine. The second **FM1** molecule formed a hydrogen bond with the tyramine hydroxyl group in this complex. Scheme 1c and 1d show the structural formula and the DFT optimized structure of

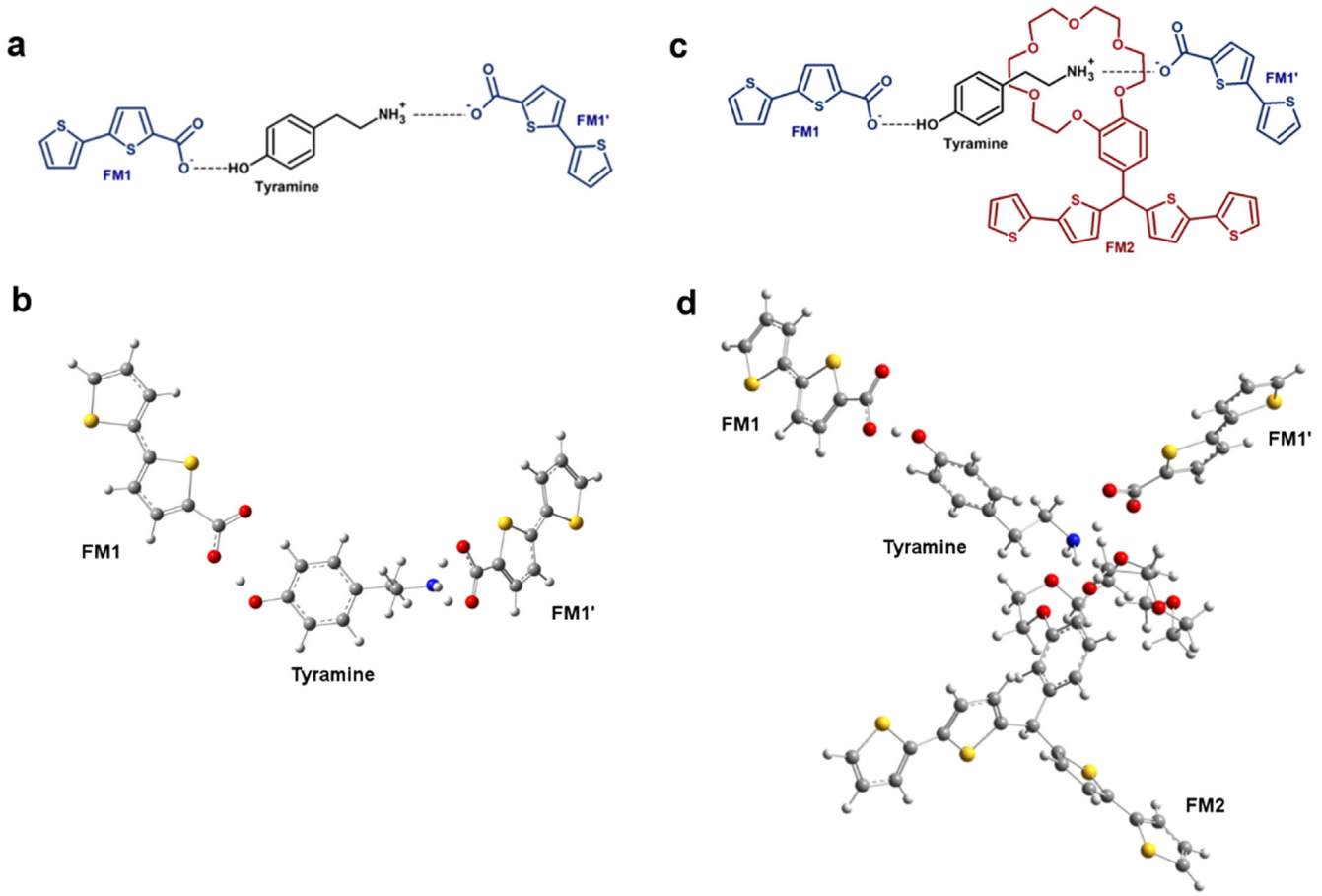

Scheme 1. (a) and (c) Structural formulas as well as (b) and (d) DFT optimized structures of the tyramine pre-polymerization complexes containing (a) and (b) two molecules of monomer **FM1** or (c) and (d) two molecules of monomer **FM1** and one molecule of the monomer **FM2**. DFT calculations were performed with the B3LYP functional and the 3–21 g(*) basis set at room temperature. The effect of the acetonitrile solvent was approximated with the PCM model.

the complex of one tyramine molecule with two molecules of the **FM1** monomer and one of the **FM2** monomer, respectively. For this complex, the calculated negative Gibbs free energy change of complex formation was much higher ΔG = -220 kJ/mol.

3.2. Simultaneous electrochemical synthesizing and depositing of MIP and NIP films

Both **MIP-1** (Fig. 1a) and **NIP-1** (Fig. 1c) films were deposited on the Pt electrodes via potentiodynamic electropolymerization. The potential was scanned from 0 to 1.30 V vs. Ag quasi-reference electrode. Five potential cycles were performed. During the deposition of each film, an anodic peak was formed at ~ 1.25 V vs. Ag quasi-reference electrode. With each consecutive potential cycle, anodic currents appeared at slightly lower potentials, and the current peaks increased, thus manifesting successful electropolymerization and simultaneous film deposition. Moreover, a cathodic peak at 1.00 V vs. Ag quasi-reference electrode emerged in the second cycle. This peak may be assigned to polythiophene cation radical electroreduction, thus additionally confirming successful film deposition. Moreover, complete coverage of the electrode surface with the **MIP-1** film was confirmed with the CV and DPV experiments in the presence of the $Fe(CN)_6^{4-}/Fe(CN)_6^{3-}$ redox probe (Figure S1 in Supplementary Material). During tyramine template extraction with 0.1 M NaOH, the current of the redox probe increased and then reached a constant value after 45 min.

Currents recorded during **MIP-2** (Fig. 1b) and **NIP-2** (Fig. 1d) film deposition resembled those for the **MIP-1** (Fig. 1a) and **NIP-1** (Fig. 1c), respectively, film deposition. However, anodic peaks of monomers electro-oxidation were slightly shifted positively, namely, to 1.30 V vs. Ag quasi-reference electrode. This shift may suggest the formation of a more stable pre-polymerization complex. Therefore, the potential was scanned from 0 to 1.40 V vs. Ag quasi-reference electrode during the electropolymerization. The **MIP-2** and **NIP-2** films deposited that way were more compact and less conductive than the **MIP-1** and **NIP-1** films. Apparently, **MIP-2** and **NIP-2** films were sufficiently thick after two potential cycles to block redox probe access to the electrode surface (Fig. 2a curve 2 and Fig. 2b curve 2′). The faradaic peak currents of the redox probe in both the CV and DPV experiments increased during tyramine extraction. After 150 min of extraction, changes in DPV curves for the redox probe recorded on the **MIP-2** film-coated electrode approached a constant value (Fig. 2a and 2b, curves 3 and 5′, respectively), thus manifesting successful extraction of the tyramine template.

3.3. AFM imaging as well as XPS and PM-IRRAS characterizing of MIP-2 and NIP-2 films

The deposited **MIP-2** and **NIP-2** films were characterized by XPS (Tables S1-S3 in Supplementary Material) and PM-IRRAS (Figure S2 in Supporting Material). Two weak bands in the PM-IRRAS spectra at ~ 3100 and ~ 2900 cm^{-1} of all deposited films may be assigned to C-H bond stretching vibration in aromatic and aliphatic moieties, respectively. Moreover, a well-pronounced band between 1750 and 1700 cm^{-1} was present in the spectra for all films. This band

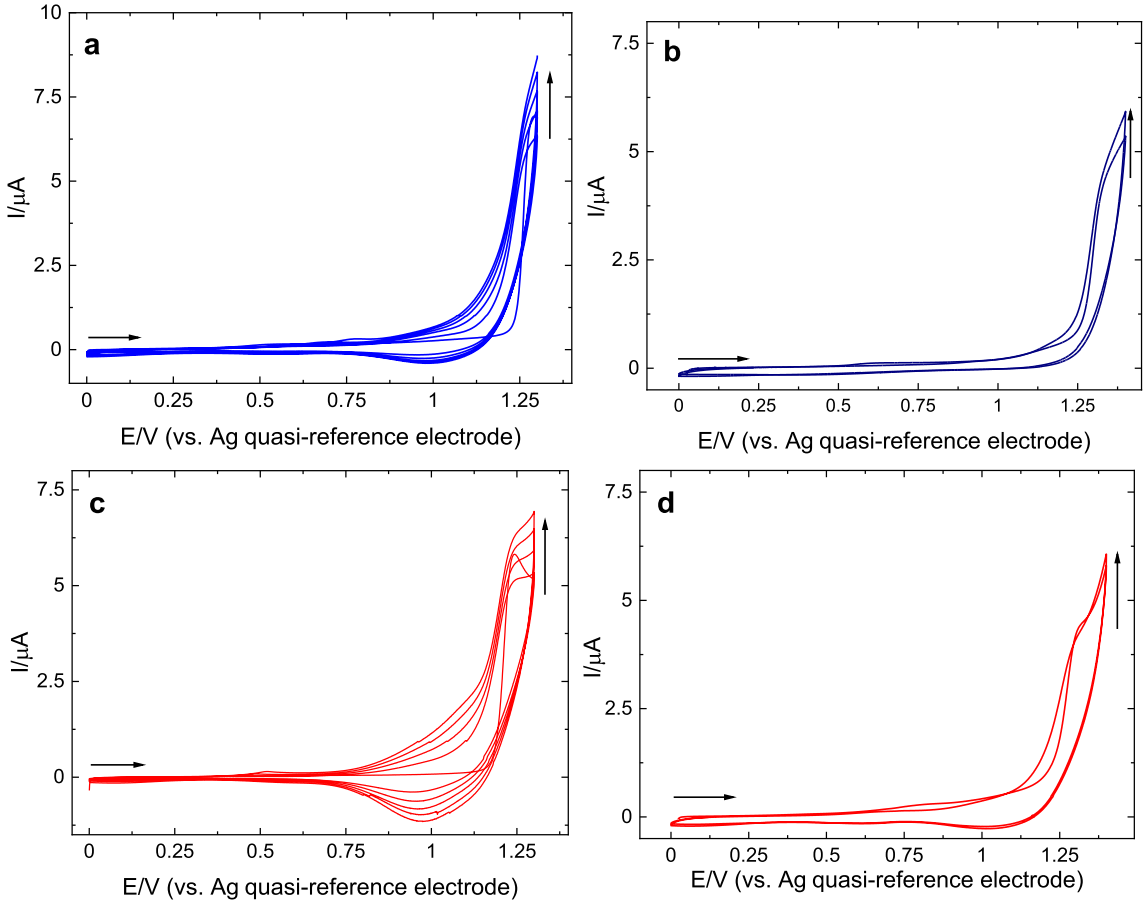

Fig. 1. Current-potential curves recorded for deposition of the (a) **MIP-1**, (b) **MIP-2**, (c) **NIP-1**, and (d) **NIP-2** films on 0.75-mm diameter Pt disk electrodes. An acetonitrile solution of (a and c) 50 μM tyramine, (a - d) 100 μM 2,2′-bithiophene-5-carboxylic acid **FM1**, (c) and (d) 50 μM **FM2**, (a - d) 500 μM 2,3′-bithiophene, and (a - d) 0.1 M (TBA) ClO_4 was used for this electropolymerization. The potential scan rate was 50 mV/s.

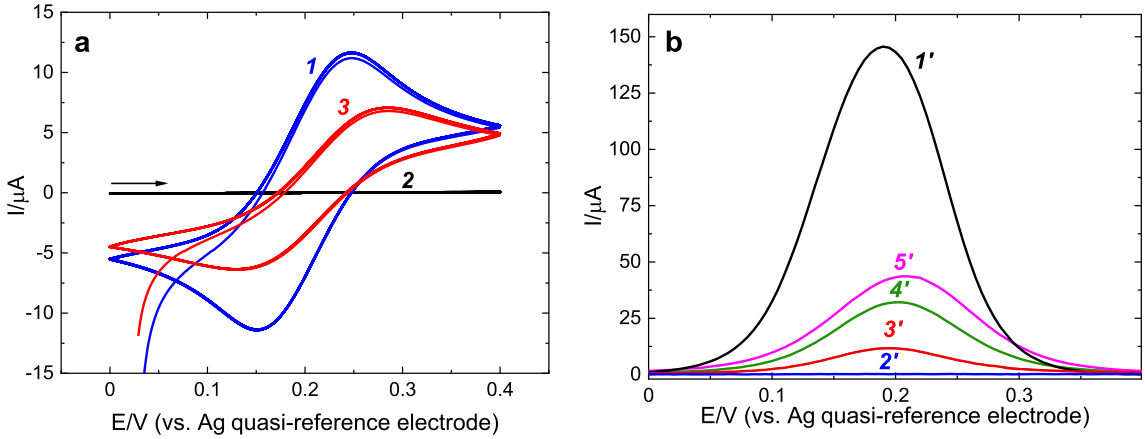

Fig. 2. (a) CV curves for 0.1 M $K_3[Fe(CN)_6]$ and 0.1 M $K_4[Fe(CN)_6]$ in PBS (pH = 7.4) on (*1*) the bare Pt electrode, as well as the **MIP-2** film-coated Pt electrode (*2*) before and (*3*) after 150-min extraction in 0.1 M NaOH. (b) DPV curves for 100 mM $K_3[Fe(CN)_6]$ and 100 mM $K_4[Fe(CN)_6]$ in 0.1 M PBS (pH = 7.4) recorded on (*1′*) the bare Pt electrode, as well as the **MIP-2** film-coated Pt electrode (*2′*) before and after (*3′*) 10, (*4′*) 60, and (*5′*) 150 min of extraction in 0.1 M NaOH.

originated from C=O bond stretching, thus confirming successful copolymerization and deposition of all monomers present in the pre-polymerization complex solution. However, the band of the N-H stretching vibration was not evident in the PM-IRRAS spectrum of **MIP-2** film before extraction. The intensity of the N-H stretching vibration signal is moderate. Moreover, the tyramine content in the deposited MIP film is low compared to the contents of the monomers. Therefore, we expect the intensity of the N-H stretching band to be relatively low. The MIP film is very thin. Thus, the signal-to-noise ratio in the recorded PM-IRRAS spectrum is low. Therefore, this band may not be visible. Moreover, protonation of the primary amine group of tyramine and complex formation of this group with the crown ether moiety of **FM2** may result in a shift of the band of the N-H stretching vibration to wavenumbers lower than expected. We may only speculate whether this band overlaps with that assigned to the C-H stretching bands in the range of 3100–3000 cm^{-1} or not.

The N1s core level XPS spectra (not presented) confirm the tyramine presence in the **MIP-2** film before extraction. Although the AFM determined film thickness, described below, was much larger than the depth of XPS sampling (1–2 nm), with the XPS technique, we could compare relative changes in elemental compositions of both MIP and NIP samples, evaluated within the same XPS sampling depth. We are aware that the composition of the surface of the deposited films is not fully representative of the composition of the bulk of polymer grains. However, the XPS data quite well confirm a change of elemental composition due to chemical treatment. The nitrogen content in both **MIP-2** and **NIP-2** films was evaluated (Tables S1-S4 in Supplementary Material). The nitrogen content in the **MIP-2** spectrum significantly decreased after the extraction of the tyramine template (Tables S1 and S2 in Supplementary Material). The N-to-C ratio dropped to only half of its original value (Table S5 in Supplementary Material). However, this drop might originate from both tyramine or/and entrapped tetrabutylammonium cation removal. Therefore, **NIP-2** film was subjected to a similar "extraction" treatment. After this treatment, the nitrogen content in the **NIP-2** film decreased only slightly. This decrease indicates that the TBA^+ removal during the extraction was negligible. Thus, the XPS data support successful tyramine removal from the film. The XPS sulfur content of 12.8 at.% slightly decreased (to 8.2 at.%) after tyramine extraction from the **MIP-2** film. We may only speculate that the **MIP-2** film treatment with a basic aqueous solution during the extraction caused a rearrangement of surface polymer chains in such a way that the hydrophilic carboxyl groups and crown ether moieties were exposed to the solution, thus hiding the hydrophobic polythiophene polymer backbone inside the grains. The decrease in the sulfur signal may also be caused by the removal from the film of oligomers and traces of unreacted monomers during the extraction.

AFM images of the polymer films are presented in Figure S6 in Supplementary Material. The determined morphological and nanomechanical parameters are summarized in Table S4 in Supplementary Material. Per the film deposition procedure, all deposited films were quite thin. The AFM determined thickness of the **MIP-2** film before template extraction was 19 (±2) nm, while the **NIP-2** film was slightly thicker, 24 (±3) nm. The removal of tyramine from the **MIP-2** film led to a minor decrease of the film thickness to 16 (±1) nm while the **NIP-2** film thickness practically remained unchanged, equalling 24 (±2) nm. Roughness (R_a) determined for the "as-deposited" polymer films was markedly higher than that for the bare gold support. Moreover, the **MIP-2** film was rougher, being 2.7 (±0.3) nm, than the **NIP-2** film, amounting to 1.9 (±0.2) nm. Interestingly, the roughness of the **NIP-2** film significantly increased while that of the **MIP-2** film decreased after tyramine extraction (Table S6 in Supplementary Material).

As expected for such thin films, the observed film topography was highly influenced by the topography of the underlying gold film. All of the films were composed of circular grains with an average diameter in the range of 40 to 70 nm. Yet, there were some differences in the morphology of the grains. That is, uneven and unsymmetrical grains looking like fused small and large grains were seen in "as-deposited" **MIP-2** and **NIP-2** films (Figure S4a and S4b, respectively, in Supplementary Material). These surface features are in contrast to quite uniform and round grains visible in images of the gold support (not shown). "Extraction" of the **NIP-2** film altered grain morphology to some extent, but the grains preserved their general features of non-extracted **NIP-2** film (Figure S4b' in Supplementary Material). On the other hand, the **MIP-2** morphology changes after tyramine extraction were more pronounced (Figure S4a' in Supplementary Material). Here, the grains were more even and globular. However, differences in the grain sizes were still much higher than those for the bare gold support. Moreover, the estimated average grain diameter for tyramine-extracted **MIP-2** (65 nm) was higher than that for the bare gold support (49 nm). The observed surface morphology changes indicate that the extraction led to the removal of these **MIP-2** film parts, which were weaker bound. However, **NIP-2** film adhesion to the gold support was stronger.

The examination of the nanomechanical properties of the polymer films confirmed that both the **MIP-2** and **NIP-2** films were

deposited, indeed. For these films, the Young modulus was in accord with that reported for polythiophene films, i.e., it was ~ 6 GPa [20,21]. This value is much lower than that of 42 GPa estimated for bare gold. The latter value should be considered as an estimation only because the tip spring constant was not adjusted for measurements of highly rigid objects. However, its magnitude well corresponds to the literature value of 69 GPa [22]. For both the **MIP-2** and **NIP-2** film, the Young modulus substantially decreased after tyramine extraction, thus indicating film "softening". Interestingly, the adhesion of the Si tip to the polymer film surface (5 to 8 nN) was much weaker than that to the bare gold support (19 nN). Considering that the Si tip is typically coated with a few nm thick film of hydrophilic silicon oxide and that the polythiophene films studied herein are relatively hydrophobic, one can easily understand this adhesion decrease. So, the nanomechanical studies performed further confirm the formation of polymer films on gold support.

Moreover, SEM imaging of deposited films showed uniform surface coating (Figure S5 in Supplementary Material).

3.4. DPV and EIS selective tyramine determining with MIP-1 and MIP-2 film-coated electrodes

The above-described **MIP-1** and **MIP-2** film-coated electrodes were applied for DPV determination of tyramine. The $Fe(CN)_6^{4-}/Fe(CN)_6^{3-}$ DPV peak current for the **MIP-1** film coated electrode linearly decreased with the increase of the tyramine concentration in the micromolar concentration range (Figure S3 in Supplementary Material). However, the **MIP-1** film-coated electrode was not selective when tested vs common interfering compounds, namely, glucose, urea, and creatinine. To incur this selectivity, we introduced additional interactions of the imprinted molecular cavities with molecules of the tyramine analyte. For that purpose, a crown-ether-moiety-containing **FM2** monomer was added to the pre-polymerization complex solution. This monomer provided an additional supramolecular site for tyramine recognition (Scheme 1c and 1d), thus improving chemosensor selectivity (Fig. 3).

The linear dynamic concentration range of the **MIP-2** film coated electrode extended from 290 μM to 2.64 mM tyramine in DPV determinations. Changes in the DPV peak current fulfilled the following linear regression equation. $(I_{DPV,0} - I_{DPV,s})$ [μA] = -0.67(±0.71) [μA] + 13.39(±0.86) [μA/mM] $c_{tyramine}$ [mM]. The correlation coefficient and the lower limit of detection at S/N = 3 was R^2 = 0.9859 and LOD = 159 μM, respectively. Moreover, a control **NIP-2** film coated electrode was applied for tyramine determination. The apparent imprinting factor, estimated from the ratio of slopes of calibration plots constructed for both electrodes, was high, IF = 5.6, thus confirming successful imprinting. The **MIP-2** chemosensor response to common interferences was examined to estimate its selectivity (Fig. 3c). The selectivity coefficient for creatinine was 17.7, and responses to changes in glucose and urea concentrations were negligible. Moreover, the selectivity to close structural tyramine analogs was studied. After the initial addition of L-tyrosine, adrenaline, or D-phenylalanine, a pronounced decrease in the DPV signal was observed. However, at their con-

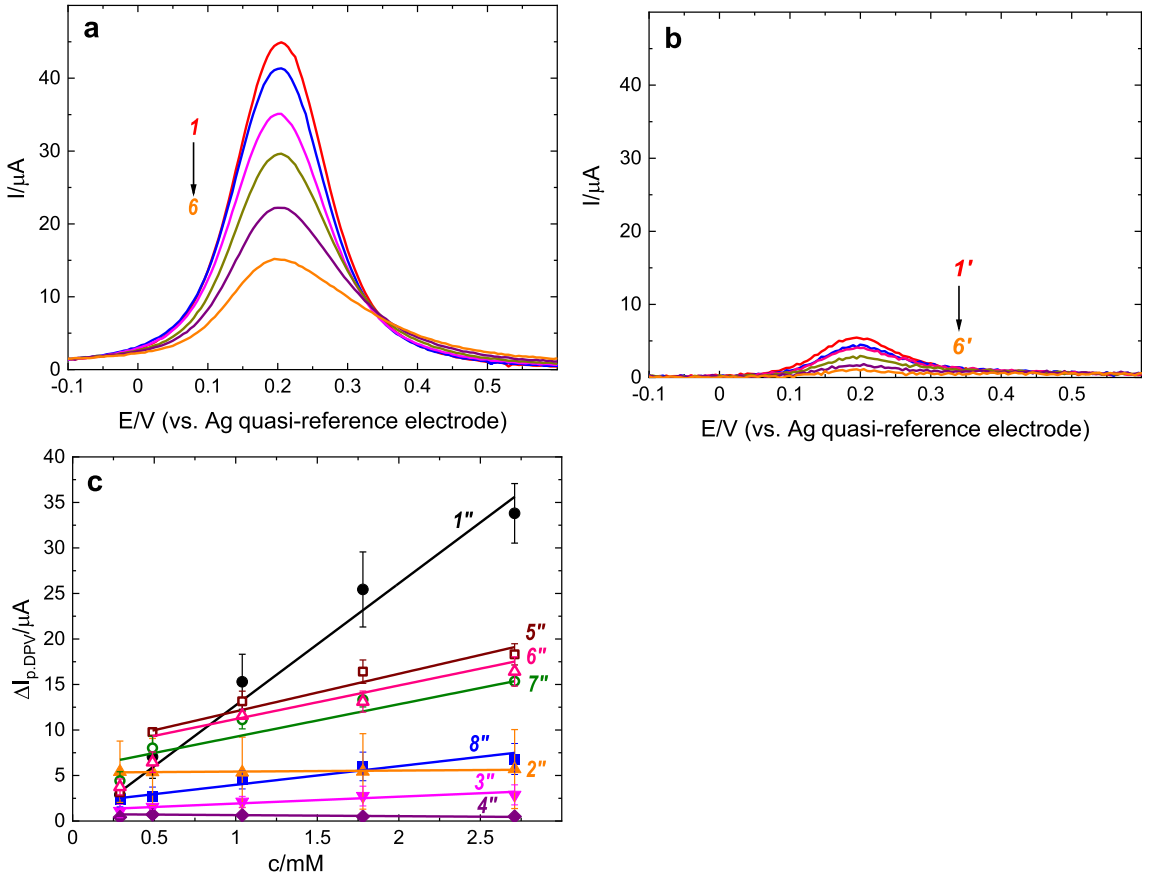

Fig. 3. DPV curves recorded for (a) **MIP-2** and (b) **NIP-2** film coated 0.75-mm diameter Pt disk electrodes (*1* and *1′*) after tyramine extraction and in the presence of (*2* and *2′*) 290 μM, (*3* and *3′*) 490 μM, (*4* and *4′*) 1.01 mM, (*5* and *5′*) 1.76 mM, or (*6* and *6′*) 2.64 mM tyramine in 0.1 M $K_3[Fe(CN)_6]$ and 0.1 M $K_4[Fe(CN)_6]$, in 0.1 M PBS (pH = 7.4). (c) Calibration plots of DPV peak current changes with the concentration change of (*1″* and *8″*) tyramine, (*2″*) glucose, (*3″*) creatinine, (*4″*) urea, (*5″*) L-tyrosine, (*6″*) adrenaline, and (*7″*) D-phenylalanine on the (*1″ – 7″*) **MIP-2** and (*5″*) **NIP-2** film coated electrode.

centrations exciding 0.5 mM, the **MIP-2** film coated electrode response to changes of concentration of these interferences was significantly lower than that of tyramine. Therefore, the calculated selectivity coefficients were 3.2, 3.8, and 3.6, respectively. Unfortunately, the chemosensor revealed no selectivity to tryptamine (data not shown).

Immediately after recording the above-discussed DPV curves, the EIS spectra were recorded, for the same solutions, to get a closer insight into mechanistic aspects of the chemosensor response [23]. Then, the Nyquist plots were constructed. In these plots, semicircles with diameters corresponding to the charge transfer resistance (R_{ct}) of the redox probe faradaic process were well pronounced (Fig. 4a). These semicircles were significantly flattened, most likely because of the inhomogeneity of the electrode surfaces. Moreover, there were straight lines in these plots in the low-frequency ranges of the spectra. These lines correspond to Warburg impedance. Slopes of these lines were slightly lower than 45° expected for fully diffusional rate control. Namely, they were equal to 37 (±2)°, thus indicating the possible influence of the **MIP-2** film properties on redox probe diffusion through the film to the electrode surface. However, these slopes were independent of the tyramine concentration. So, the **MIP-2** film neither swelled nor contracted as a result of analyte binding. Evidently, the chemosensor response originated from changes in **MIP-2** conductivity [23]. This inference was supported by Bode plots, where only one peak in the frequency range of 1 to 10 kHz was present (Fig. 4b). The

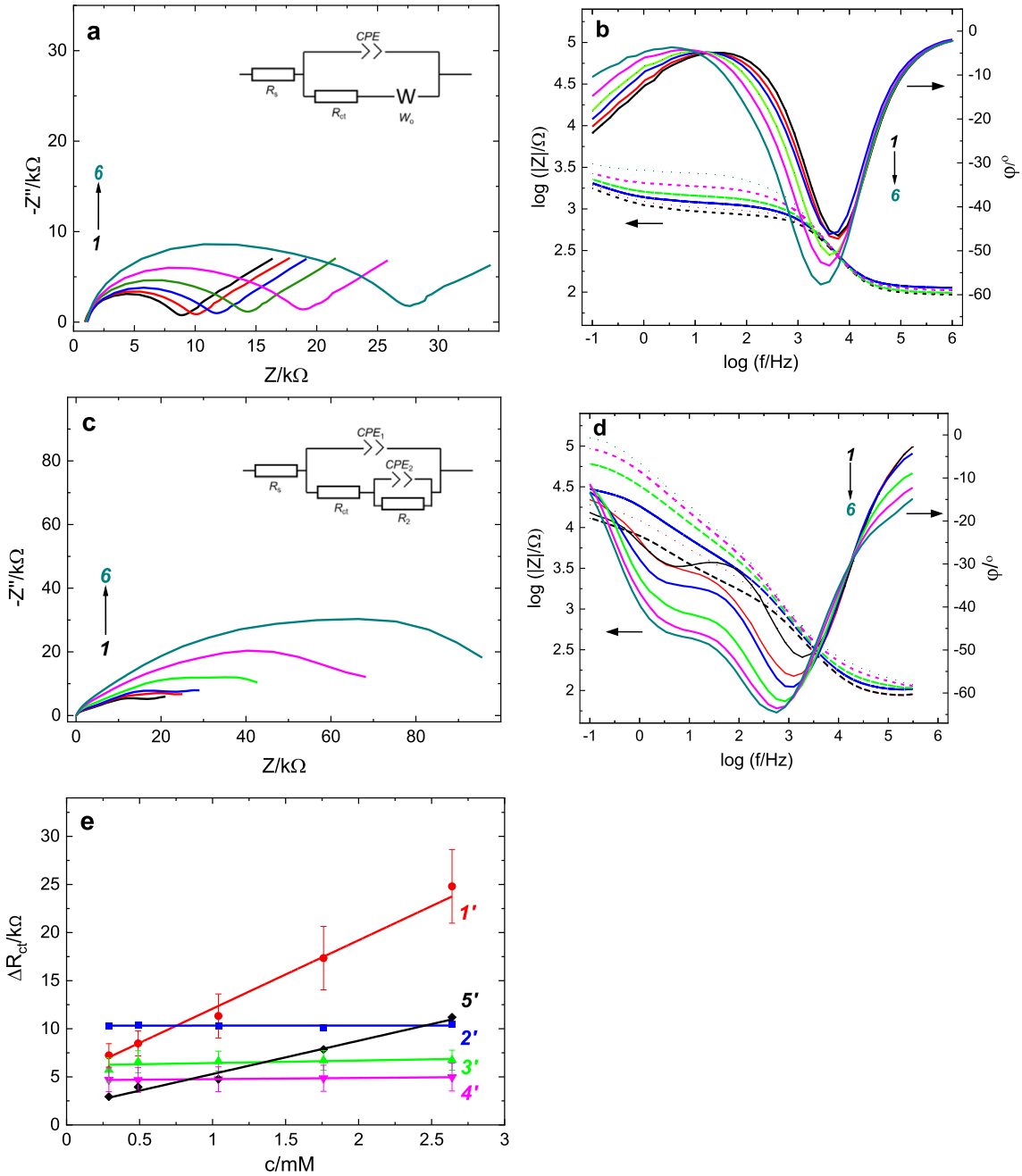

Fig. 4. The (a and c) Nyquist and (b and d) Bode plots for 0.75-diameter Pt disk electrodes coated with the (a and b) **MIP-2** and (c and d) **NIP-2** film and immersed in 0.1 M $K_3[Fe(CN)_6]$ and 0.1 M $K_4[Fe(CN)_6]$, in 0.1 M PBS (pH = 7.4) (*1*) after tyramine extraction, and then (*2*) in the presence of 290 μM, (*3*) 490 μM, (*4*) 1.04 mM, (*5*) 1.76 mM, or (*6*) 2.64 mM tyramine. (e) Calibration plots of the charge transfer resistance change with the change of concentration of (*1′*) tyramine, (*2′*) urea, (*3′*) glucose, and (*4′*) creatinine on the tyramine-extracted **MIP-2** film coated electrode as well as (*5′*) tyramine on the **NIP-2** film coated electrode. Equivalent circuits fitted to the EIS spectra for (a, insert) **MIP-2** and (c, insert) **NIP-2** film-coated electrodes.

electrochemical system was approximated with a modified Randles-Ershler equivalent circuit, $R_s + CPE/(R_{ct} + W_o)$, where R_s, R_{ct}, *CPE*, and W_o are solution resistance, charge transfer resistance, constant phase element, and Warburg impedance, respectively. The R_{ct} changes were linearly dependent on the tyramine concentration from 290 μM up to 2.64 mM (Fig. 4e). These changes obeyed the following linear regression equation. (R_{ct}) [kΩ] = 4.97 (±0.38) [kΩ] + 7.11 (±0.45) [kΩ/mM] $c_{tyramine}$ [mM]. The correlation coefficient and the lower limit of detection at S/N = 3 was R^2 = 0.9843 and LOD = 168 μM tyramine, respectively. The coefficient of selectivity to creatinine was 28, and the **MIP-2** chemosensor responded neither to changes of glucose nor urea concentrations.

Significantly, the EIS spectra recorded for the control **NIP-2** film-coated electrodes (Fig. 4c and 4d) differed from those for the **MIP-2** film-coated electrodes (Fig. 4a and 4b). That is, only tiny initial parts of semicircles with diameters determining R_{ct} values were developed in a high-frequency range of the Nyquist plots (Fig. 4c). The size and shape of these semicircle parts depended on the tyramine concentration. These parts were followed by relatively flat and slightly curved lines, apparently forming other huge semicircles. Those may be assigned to redox probe diffusion through the porous non-conductive **NIP-2** film. The diameter of the second semicircle increased with the increase of the tyramine concentration.

Moreover, there were two peaks in the Bode plots (Fig. 4d). One, at high frequencies, corresponded to a faradaic process of the redox probe. The other, in the frequency range of 1 to 10 Hz, could originate from redox probe diffusion through the porous polymer film [24–27]. This peak was absent in the spectra recorded for the **MIP-2** film-coated electrode (Fig. 4b). Evidently, the mechanisms of the electrochemical response at the **NIP-2** and **MIP-2** film-coated electrodes were different. For the **NIP-2** film-coated electrode, a "gate effect" mechanism is operative [19]. This mechanism assumes that the electrode is coated with a non-conductive porous polymer film and that a redox probe diffuses through pores of this film to the electrode surface for charge exchange.

Analyte ingress to the film causes film swelling or shrinking and, hence, expansion or contraction, respectively, of the pores. Therefore, the redox probe diffusion trough these pores is affected. Thus, it was not possible to fit the Randles-Ershler equivalent circuit (Fig. 4a, insert) to the EIS spectra recorded for the **NIP-2** film coated electrode. Instead, the circuit shown in Fig. 4c fitted quite well [24–27]. From the ratio of slopes of the R_{ct} changes of **MIP-2** and **NIP-2** film-coated electrodes with the tyramine concentration changes, we estimated the apparent imprinting factor as *IF* = 2.1. This relatively low IF value may result from fitting different equivalent circuits to Nyquist plots to determine the R_{ct} values for the **MIP-2** and **NIP-2** film-coated electrodes. Thus, the calculated IF value reliability is limited.

3.5. Applying MIP-2 film-coated electrodes for DPV tyramine determining in real samples

The devised **MIP-2** chemosensor was applied for tyramine DPV determination in samples of Mozzarella cheese whey. This determination highlights its usefulness for tyramine quantitation in real samples. As shown in Fig. 5, the matrix effect was quite pronounced. That is, the recorded signal changes after initial sample injections were higher than those in the blank 0.1 M PBS (pH = 7.4) solution. Moreover, for tyramine concentrations exceeding 1 mM, the **MIP-2** film was saturated with tyramine. Hence, it was not possible to apply the same linear calibration plot as that for the determination of tyramine in the PBS solution. Therefore, the three most commonly used isotherms, namely, the Langmuir, Freundlich, and Langmuir-Freundlich isotherms, were fitted to the data acquired (Fig. 5 and Table 2) [28–31]. Evidently, the

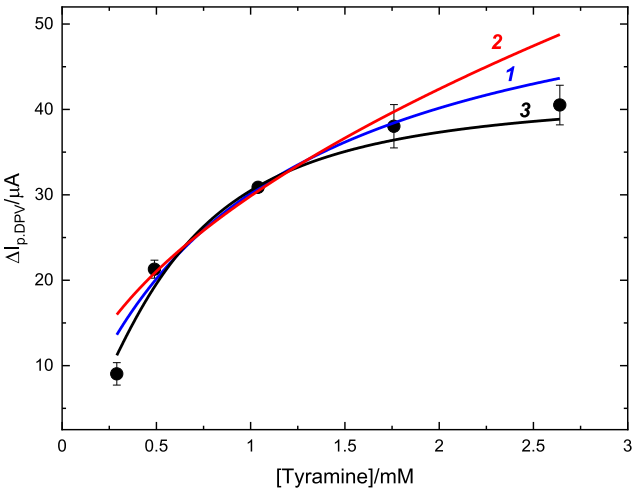

Fig. 5. (*1*) Langmuir, (*2*) Freundlich, and (*3*) Langmuir-Freundlich isotherm fitting to the DPV peak current change with the tyramine concentration change in real samples of Mozzarella cheese whey. DPV measurements were performed for the tyramine-extracted **MIP-2** film-coated 0.75-mm diameter Pt disk electrodes using 0.1 M $K_3[Fe(CN)_6]$ and 0.1 M $K_4[Fe(CN)_6]$ in Mozzarella cheese whey diluted 100 times with 0.1 M PBS (pH = 7.4).

Langmuir-Freundlich isotherm (Fig. 5, curve 3) fitted best. Therefore, this isotherm was used as the calibration plot for tyramine in whey samples. Four Mozzarella whey samples were spiked with tyramine, and then the tyramine concentration in these samples was determined with freshly prepared **MIP-2** film-coated electrodes (Table 3). The recovery obtained was acceptable, thus suggesting that the selectivity of the chemosensor was sufficiently high for tyramine determination in food samples. However, additional sample purifying or constructing a separate calibration plot for each matrix is recommended. We may only speculate if this behavior originates from higher ionic strength of whey samples or other effects.

4. Conclusions

An MIP film based electrochemical sensor for selective determination of tyramine was devised, fabricated, and tested. The structure of the tyramine template pre-polymerization complex with two different functional monomers was optimized with DFT modeling. A chemosensor pronounced detectability was due to tyramine accumulation in the MIP film. That resulted in the amplification of the detection signal. The introduction to the molecularly imprinted cavities of an additional supramolecular site for tyramine recognition, namely, a crown ether moiety of functional monomer **FM2**, significantly increased the chemosensor selectivity. The **MIP-2** chemosensor linear dynamic concentration range in both differential pulse voltammetry (DPV) and electrochemical impedance spectroscopy (EIS) determinations, with the use of the $Fe(CN)_6^{4-}/Fe(CN)_6^{3-}$ redox probe, covered the micro- and millimolar tyramine concentration ranges. The limit of detection at S/N = 3 for DPV and EIS determinations was 159 and 168 μM tyramine, respectively. Moreover, there was a substantial difference in the performance of the MIP and NIP film-coated electrodes. This difference was unraveled by the EIS detailed study of the electrochemical sensor response mechanism.

Declaration of Competing Interest

The authors declare that they have no known competing financial interests or personal relationships that could have appeared to influence the work reported in this paper.

Table 2
Results of isotherm fitting to the DPV peak current changes with the tyramine concentration change in real samples of Mozzarella cheese whey measured with **MIP-2** film-coated 0.75-mm diameter Pt disk electrodes.

Isotherm	Isotherm equation	Fitted parameters			R^2
		$\Delta I_{DPV,max}$, μA	K, mM^{-1}	n	
Langmuir	$\Delta I_{DPV} = \Delta I_{DPV,max} \frac{K_L c_{tyramine}}{1+K c_{tyramine}}$	60.0 (±10.7)	1.01[a] (±0.366)	–	0.9555
Freundlich	$\Delta I_{DPV} = K_F c_{tyramine}^{\frac{1}{n}}$	–	29.86[b] (±1.00)	1.96[d] (±0.12)	0.8794
Langmuir-Freundlich	$\Delta I_{DPV} = \Delta I_{DPV,max} \frac{(K_{LF} c_{tyramine})^n}{1+(K_{LF} c_{tyramine})^n}$	41.9 (±7.3)	1.84[c] (±0.478)	1.61[e] (0.467)	0.9786

[a] K_L - Langmuir constant
[b] K_F - Freundlich constant
[c] K_{LF} - Langmuir-Freundlich constant
[d] Adsorption intensity
[e] Homogeneity factor

Table 3
Results of tyramine determination in Mozzarella whey samples with the **MIP-2** film-coated electrode using the Langmuir-Freundlich fitted isotherm as the calibration plot.

Sample No.	Concentration of added tyramine, mM	ΔI_{DPV}, μA	Calculated tyramine concentration, mM	Recovery, %
1	0.3	9.54 (±2.64)	0.25 (±0.10)	84.8 (±33.9)
2	0.4	15.68 (±2.86)	0.39 (±0.11)	98.7 (±26.8)
3	0.5	21.83 (±3.62)	0.57 (±0.13)	115.0 (±25.1)
4	0.6	23.70 (±0.76)	0.64 (±0.05)	107.0 (±7.6)

Acknowledgments

The authors thank Jakub Kalecki for SEM imaging of the deposited polymer films. The present research was financially supported by the Polish National Science Foundation (NCN) through Grant No. 2014/15/B/NZ7/01011 to WK. Moreover, this scientific work was funded from the financial resources for science in the years of 2017-2021, awarded by the Polish Ministry of Science and Higher Education for the implementation of an international co-financed project. Furthermore, the present publication is part of a project that has received funding from the European Union's Horizon 2020 research and innovation program under the Marie Sklodowska-Curie grant agreement No. 711859. FD is thankful to UNT-AMMPI for financial support.

Appendix A. Supplementary data

Supplementary data to this article can be found online at https://doi.org/10.1016/j.bioelechem.2020.107695.

References

[1] L.V. Jorgensen, H.H. Huss, P. Dalgaard, The effect of biogenic amine production by single bacterial cultures and metabiosis on cold-smoked salmon, J Appl Microbiol 89 (6) (2000) 920–934, https://doi.org/10.1046/j.1365-2672.2000.01196.x.
[2] VikramK Yeragani, T.S. Sathyanarayana Rao, Hypertensive crisis and cheese, Indian J Psychiatry 51 (1) (2009) 65, https://doi.org/10.4103/0019-5545.44910.
[3] L.F. Blob, M. Sharoky, B.J. Campbell, E.M. Kemper, M. Gilmor, C.M. VanDenBerg, A.J. Azzaro, Effects of a Tyramine-Enriched Meal on Blood Pressure Response in Healthy Male Volunteers Treated with Selegiline Transdermal System 6 mg/24 Hour, CNS spectr. 12 (1) (2007) 25–34, https://doi.org/10.1017/S1092852900020496.
[4] K. Holden, Meal ideas and menus: Avoiding high-tyramine foods made easy, Teva Neuroscience Inc. 2006.
[5] P.S. Sharma, Z. Iskierko, A. Pietrzyk-Le, F. D'Souza, W. Kutner, Bioinspired intelligent molecularly imprinted polymers for chemosensing: A mini review, Electrochemistry Communications 50 (2015) 81–87, https://doi.org/10.1016/j.elecom.2014.11.019.
[6] M. Cieplak, W. Kutner, Artificial biosensors: How can molecular imprinting mimic biorecognition?, Trends Biotechnol. 34 (2016) 922–941.
[7] N.F. Atta, M.M. Hamed, A.M. Abdel-Mageed, Computational investigation and synthesis of a sol–gel imprinted material for sensing application of some biologically active molecules, Analytica Chimica Acta 667 (1-2) (2010) 63–70, https://doi.org/10.1016/j.aca.2010.04.005.
[8] N.F. Atta, A.M. Abdel-Mageed, Smart electrochemical sensor for some neurotransmitters using imprinted sol–gel films, Talanta 80 (2) (2009) 511–518, https://doi.org/10.1016/j.talanta.2009.07.014.
[9] J. Huang, X. Xing, X. Zhang, X. He, Q. Lin, W. Lian, H. Zhu, A molecularly imprinted electrochemical sensor based on multiwalled carbon nanotube-gold nanoparticle composites and chitosan for the detection of tyramine, Food Research International 44 (1) (2011) 276–281, https://doi.org/10.1016/j.foodres.2010.10.020.
[10] Q. Wang, D. Zhang, A novel fluorescence sensing method based on quantum dot-graphene and a molecular imprinting technique for the detection of tyramine in rice wine, Anal. Methods 10 (31) (2018) 3884–3889, https://doi.org/10.1039/C8AY01117F.
[11] D. Zhang, H. Liu, W. Geng, Y. Wang, A dual-function molecularly imprinted optopolymer based on quantum dots-grafted covalent-organic frameworks for the sensitive detection of tyramine in fermented meat products, Food Chemistry 277 (2019) 639–645, https://doi.org/10.1016/j.foodchem.2018.10.147.
[12] J.-D. Lee, J.-I. Hong, Two-dimensional sensor array for discrimination of amines, Tetrahedron Letters 54 (22) (2013) 2890–2893, https://doi.org/10.1016/j.tetlet.2013.03.118.
[13] P. Lulinski, M. Sobiech, T. Zolek, D. Maciejewska, A separation of tyramine on a 2-(4-methoxyphenyl)ethylamine imprinted polymer: An answer from theoretical and experimental studies, Talanta 129 (2014) 155–164.
[14] Y. Li, C.H. Hsieh, C.W. Lai, Y.F. Chang, H.Y. Chan, C.F. Tsai, J.A. Ho, L.C. Wu, Tyramine detection using PEDOT:PSS/AuNPs/1-methyl-4-mercaptopyridine modified screen-printed carbon electrode with molecularly imprinted polymer solid-phase extraction, Biosens. Bioelectron. 87 (2017) 142–149.
[15] M. Liu, B. Zhang, M. Zhang, X. Hu, W. Chen, G. Fang, S. Wang, A dual-recognition molecularly imprinted electrochemiluminescence sensor based on g-C_3N_4 nanosheets sensitized by electrodeposited rGO-COOH for sensitive and selective detection of tyramine, Sensor. Actuat. B-Chem. 311 (2020) 127901.
[16] P.S. Sharma, A. Garcia-Cruz, M. Cieplak, K.R. Noworyta, W. Kutner, 'Gate effect' in molecularly imprinted polymers: the current state of understanding, Current Opinion in Electrochemistry 16 (2019) 50–56, https://doi.org/10.1016/j.coelec.2019.04.020.
[17] A. Pietrzyk, S. Suriyanarayanan, W. Kutner, R. Chitta, F. D'Souza, Selective Histamine Piezoelectric Chemosensor Using a Recognition Film of the Molecularly Imprinted Polymer of Bis(bithiophene) Derivatives, Anal. Chem. 81 (7) (2009) 2633–2643, https://doi.org/10.1021/ac8025652.
[18] M. Dabrowski, M. Cieplak, P.S. Sharma, P. Borowicz, K. Noworyta, W. Lisowski, F. D'Souza, A. Kuhn, W. Kutner, Hierarchical templating in deposition of semi-covalently imprinted inverse opal polythiophene film for femtomolar determination of human serum albumin, Biosensors and Bioelectronics 94 (2017) 155–161, https://doi.org/10.1016/j.bios.2017.02.046.
[19] Y. Yoshimi, R. Ohdaira, C. Iiyama, K. Sakai, "Gate effect" of thin layer of molecularly-imprinted poly(methacrylic acid-co-ethyleneglycol dimethacrylate), Sensors and Actuators B: Chemical 73 (1) (2001) 49–53, https://doi.org/10.1016/S0925-4005(00)00671-7.
[20] M.M.P. Madrigal, M.I. Giannotti, G. Oncins, L. Franco, E. Armelin, J. Puiggali, F. Sanz, L.J. del Valle, C. Aleman, Bioactive nanomembranes of semiconductor polythiophene and thermoplastic polyurethane: thermal, nanostructural and nanomechanical properties, Polym. Chem. 4 (2013) 568–583.

[21] D. Tahk, H.H. Lee, D.-Y. Khang, Elastic Moduli of Organic Electronic Materials by the Buckling Method, Macromolecules 42 (18) (2009) 7079–7083, https://doi.org/10.1021/ma900137k.
[22] M.C. Salvadori, I.G. Brown, A.R. Vaz, L.L. Melo, M. Cattani, Measurement of the elastic modulus of nanostructured gold and platinum thin films, Phys. Rev. B 67 (2003) 153404.
[23] P. Lach, M. Cieplak, M. Majewska, K.R. Noworyta, P.S. Sharma, W. Kutner, "Gate Effect" in p-Synephrine Electrochemical Sensing with a Molecularly Imprinted Polymer and Redox Probes, Anal. Chem. 91 (2019) 7546–7553.
[24] P. Leuaa, D. Priyadarshani, A.K. Tripathi, M. Neergat, Internal and External Transport of Redox Species across the Porous Thin-Film Electrode/Electrolyte Interface, J. Phys. Chem. C 123 (35) (2019) 21440–21447, https://doi.org/10.1021/acs.jpcc.9b02795.s001.
[25] S. Omanovic, S.G. Roscoe, Electrochemical Studies of the Adsorption Behavior of Bovine Serum Albumin on Stainless Steel, Langmuir 15 (23) (1999) 8315–8321, https://doi.org/10.1021/la990474f.
[26] S. Omanovic, S.G. Roscoe, Interfacial behavior of beta-lactoglobulin at a stainless steel surface: An electrochemical impedance spectroscopy study, J. Colloid. Interf. Sci. 227 (2000) 452–460.
[27] J. Bisquert, G. Garcia-Belmonte, F. Fabregat-Santiago, P.R. Bueno, Theoretical models for ac impedance of finite diffusion layers exhibiting low frequency dispersion, Journal of Electroanalytical Chemistry 475 (2) (1999) 152–163, https://doi.org/10.1016/S0022-0728(99)00346-0.
[28] R.J. Umpleby, S.C. Baxter, Y. Chen, R.N. Shah, K.D. Shimizu, Characterization of Molecularly Imprinted Polymers with the Langmuir−Freundlich Isotherm, Anal. Chem. 73 (19) (2001) 4584–4591, https://doi.org/10.1021/ac0105686.
[29] E. Turiel, C. Perez-Conde, A. Martin-Esteban, Assessment of the cross-reactivity and binding sites characterisation of a propazine-imprinted polymer using the Langmuir-Freundlich isotherm, Analyst 128 (2) (2003) 137–141, https://doi.org/10.1039/b210712k.
[30] G.P. Jeppu, T.P. Clement, A modified Langmuir-Freundlich isotherm model for simulating pH-dependent adsorption effects, Journal of Contaminant Hydrology 129-130 (2012) 46–53, https://doi.org/10.1016/j.jconhyd.2011.12.001.
[31] N. Ayawei, A.N. Ebelegi, D. Wankasi, Modelling and Interpretation of Adsorption Isotherms, Journal of Chemistry 2017 (2017) 1–11, https://doi.org/10.1155/2017/3039817.